ISSN 1392 - 1207. MECHANIKA. 2007. Nr.1(63)

Evaluation of friction due to deformed behaviour of rail in the electromagnetic railgun: numerical investigation

L. Tumonis*, R. Kačianauskas, A. Kačeniauskas*****
**Vilnius Gediminas Technical University, Saulėtekio 11, 10223 Vilnius, Lithuania, E-mail: tumonis.l@centras.lt*
***Vilnius Gediminas Technical University, Saulėtekio 11, 10223 Vilnius, Lithuania, E-mail: rkac@fm.vtu.lt*
****Vilnius Gediminas Technical University, Saulėtekio 11, 10223 Vilnius, Lithuania, E-mail: arnka@fm.vtu.lt*

1. Introduction

Rail guns have the potential to accelerate the projectiles up to velocities of 7 km/s and their great technical applications can be expected during next decade. The accelerations needed to attain these velocities, however, demand high currents generating high magnetic fields and very large Lorentz forces acting on the projectile. The gun is composed of two rails, the projectile and an energy source closed to the electric circuit. The rails guide the projectile and provide current to the brush in the projectile [1-5]. The basic construction of the rail gun is illustrated in Fig. 1. Enormous current densities, heat generation, high velocities and friction forces coupled with the dynamical interaction at the rail surface present a great challenge to all scientists working in this interdisciplinary research area.

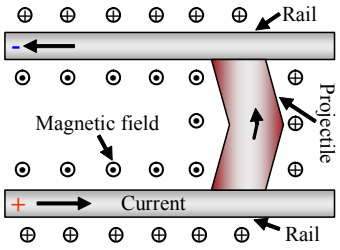

Fig. 1 Basic scheme of the rail gun

Since 1983 basic research on rail guns has been conducted at the Technical University München using experimental facilities developed for the coaxial plasmadynamic accelerator [4]. The experiments have been conducted to study the mechanical friction, the viscous arc drag and the ablation effects. At the beginning of 1987 the French-German research institute of Saint-Louis (ISL) started its activities on electro-magnetic acceleration. ISL has conducted research works on different kinds of fuse armatures for electromagnetic rail launchers [5]. In articles [6, 7], the influence of an armature material on acceleration dynamics has been investigated by means of computational methods. An accurate finite element analysis of magnetic field can be very beneficial in electromagnetic actuator design [8].

The experimental practice [9] showed that non-arcing acceleration of projectiles up to 1.1 km/s is not extraordinary. The projectiles have been accelerated without contact transition up to 2 km/s in rail guns with medium calibre (40 mm) [10]. J. Gallant and P. Lehmann [11] have presented results proving that the combination of rail gun augmentation and multibrush projectiles can lead to a higher velocity without transition in small calibre rail guns (15 mm). The problems of structural mechanics in electromagnetic rail guns have been studied by J.T. Tzeng [12]. The transient elastic waves in the rails of the electromagnetic launchers have been investigated in [13]. At present time, the research on the electromagnetic launchers as linear electromagnetic actuators has been performed at the Vilnius High Magnetic Field Centre [14].

On the basis of existing practice one can conclude that fundamental theoretical issues have been solved and several electromagnetic rail gun systems have been designed [11]. The generation and control of electromagnetic force driving the projectile may be considered as the most successful part of the above system. The question concerning efficiency of the rail gun systems is still open and many theoretical details require careful examination and revaluation.

In electromagnetic rail guns, however, there are many other physical phenomena, which are not yet clearly understood. It is not known, for example, how to precisely evaluate the friction force on the rail-projectile contact. Comprehensive low speed electric brush test data and sliding friction data for melting solids are available in the literature [1], however, only a few sources of armature test data exist [2, 3]. J.P. Barber and A. Challita [15] have been reported that the friction losses are about 5% of the electrical losses at the velocity equal 3 km/s. The significant increase of friction losses equal to 20% has been observed at 5 km/s. It is only known that the friction force strongly depends on deformations of the rails as well as on their oscillation character. Thus, it is very important to perform qualitative and quantitative investigation of friction phenomena at the rail-projectile contact and to evaluate the influence of main rail gun parameters to friction loses.

This paper is aimed to evaluate influence of the deformation behaviour of rail to friction. The integral displacement based friction ratio factor as friction indicator is suggested and examined numerically. The dynamical analysis of the rail has been performed by the finite element method. The dependency of friction ratio on the velocity of the moving load has been obtained. An outline of the paper is as follows. Section 2 describes the modelling approach including evaluation of friction factors and computation of deformation area. Section 3 presents the description of the rail gun problem. Numerical results are discussed in section 4. Conclusions are drawn in section 5.

2. Modelling approach

The modelling approach proposed here is aimed to capture an influence of the sliding brush friction increased during deformation of the rail. The main focus is to reflect this phenomenon by the friction ratio factor in terms

of deformation area of the rail. The brush contact as uncoupled rail-projectile contact is considered, where deformation of the rail occurs due to moving loading related with the position of the projectile. Finally, the loading may be defined by normal pressure q or resultant force F_N.

2.1. Friction force

In general, regardless to details of its physical nature, the friction could depend on several parameters: relative velocity, normal pressure at the rail-projectile contact and even environmental factors. Considering static friction, the tangential force is defined by Coulomb law

$$F_{f.s} = \mu_s F_{R.s} \tag{1}$$

here μ_s is static friction coefficient, which is treated as constant; $F_{R.s}$ is static normal reaction force.

In the absence of interaction effects, static reaction force $F_{R.s}$ is equal to the normal component of external force F_N acting on the projectile

$$F_{f.s} = \mu_s F_N \tag{2}$$

Here, normal force F_N present electromagnetic transversal load controlled during a shot of the rail gun.

In the dynamic analysis, the tangential friction force $F_{f.d}$ varies in time, thus it is also proportional to the dynamic normal reaction force $F_{R.d}(t)$ or

$$F_{f.d}(t) = \mu(v(t))F_{R.d}(t) \tag{3}$$

but the coefficient μ depends on projectile velocity v and materials [11]. Some data of the friction coefficient at lower velocities can be found in the literature [2, 4], but μ has not been determined yet for rail-projectile contact at the high velocities that are typical for rail guns. After making several assumptions [11], the friction coefficient is assumed to become equal constant μ_d, as soon as the projectile gains velocity. In this work, the Eq. (3) is simplified, taking into account the high velocity of the projectile:

$$F_{f.d}(t) = \mu_d F_{R.d}(t) \tag{4}$$

This expression will be explored in the development of dynamic friction.

2.2. Relative friction ratio factor

In this work, the relative dynamic friction ratio factor is proposed in order to investigate the character of friction force at the contact related to rail deformation

$$\eta = \frac{F_{f.d}}{F_{f.s}} \tag{5}$$

This factor evaluates the ratio between dynamical friction force (4) and statical friction force (1). It is indirectly assumed, that static friction phenomenon is related to undeformed state of the rail, while dynamic phenomenon is reflected by time dependent deformed behaviour of the rail. This ratio has clear physical meaning when $\eta \geq 0$ and can be computed numerically. The dynamic normal reaction force is expressed by integrating the normal contact stresses σ_N

$$F_{R.d}(t) = \int_0^{S_p} \sigma_N(x,y,t)dS \tag{6}$$

here S_p stands for contact area of the projectile. In the case of linear elastic behaviour, the normal stresses are

$$\sigma_N = Ku_N \tag{7}$$

here K is stiffness coefficient.

By assuming plane problem, the contact stress is treated as being constant across the rail width b. Thus, Eq. (6) can be rewritten as follows

$$F_{R.d}(t) = Kb\int_0^{Lq} u_N(x,t)dx \tag{8}$$

or

$$F_{R.d}(t) = KbS(t) \tag{9}$$

here S is effective area of deformation; L_q is the projectile length (Fig. 3, b). The proposed new parameter $S(t)$ is termed hereafter as deformation area of the rail

$$S(t) = \int_0^{L_q} u_N(x,t)dx$$

Substituting Eq. (2), (3) and (9) into (5), the formula for relative friction factor is obtained

$$\eta(t) = \kappa S(t) \tag{10}$$

Here

$$\kappa = \frac{\mu_d}{\mu_s}\frac{Kb}{F_N} \tag{11}$$

is proportionality factor. The Eq. (10) proves that $\eta(t)$ is proportional to the deformation area $S(t)$. Thus, the relative friction factor evaluates the reaction force at the contact, roughness of the surface, its deformation rate and the velocity of the moving load.

2.3. Computation of deformation area

Deformation area S is a very important factor, which evaluates the contact area of rail-projectile contact as well as the normal reaction force. There are several ways how to compute $S(t)$ with differently predefined contact displacement fields. Physically each version reflects different deformation energy modes. The most of them are defined by different normal displacement computing formulas. The first approach takes into account all values of the normal contact displacement u_y

$$u_N = u_y \tag{12}$$

here $u_y = u_y(x,t)$ stands for contact displacement of contact surface points x. This approach may be termed as the total contact deformation energy approach.

In Eq. (10) employing expression (12) part of the area can become negative. This total energy approach provides lower values of friction ratio. Formula (12) can be used only for illustrative purposes as an indicator of violation of the condition $S(t) \geq 0$.

Authors proposed another formula for normal displacement computations

$$u_N = \begin{cases} 0, \text{if } u_y \geq 0 \\ u_y, \text{if } u_y < 0 \end{cases} \tag{13}$$

This approach termed hereafter as full contact approach takes into account entire contact and is better suited for brush contact.

The third approach takes only collising bilateral contact displacements resisting theoretical motion of the projectile

$$u_N = \begin{cases} 0, \text{if } u_y \geq 0 \\ u_y, \text{if } u_y < 0 \text{ and } du_y / dx < 0 \end{cases} \tag{14}$$

This approach termed hereafter as partial contact approach is analogous to bilateral surface contact and would be better suited for purely mechanical contact. Graphical illustration of the proposed deformation areas is presented in (Fig. 2).

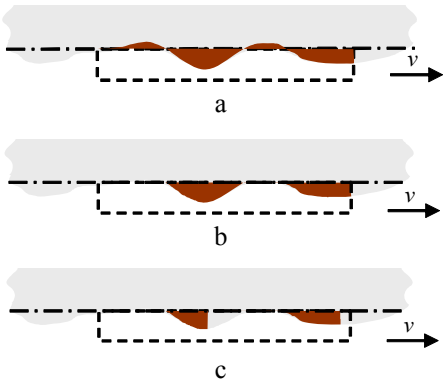

Fig. 2 Deformation areas computed by using three different formulas for stresses: a – total energy model, formula (12); b – brush friction, formula (13); c – surface friction, formula (14)

2.4. Numerical model

Dynamical behaviour of the rail is governed by linear mechanical model

$$[\boldsymbol{M}]\ddot{\boldsymbol{u}} + [\boldsymbol{K}]\boldsymbol{u} = \boldsymbol{F}_N(t)$$

Where, $\boldsymbol{u}$ is unknown nodal values of the time dependent displacement vector; $\ddot{\boldsymbol{u}}$ is acceleration; $[\boldsymbol{K}]$ is linear stiffness matrix; $[\boldsymbol{M}]$ is mass matrix; $\boldsymbol{F}_N(t)$ is vector of external time-depent electromagnetic load. The damping term is not considered in this equation, therefore, over-estimated dynamic effects are obtained. The numerical analysis of this mechanical model is performed by the finite element method software ANSYS [16].

3. Problem description

3.1. Rail geometry and material data

Computational model of the rail gun is illustrated in Fig. 3. The rail is considered as 2D domain, while connection bolts are modelled as elastic springs. Fig. 3, a shows geometry and supports. L is length of the rail. h_r is height of the rail. The rail is of the square, thus the rail width $b = h_r = 5$ cm. Distance between supports $d_s = 15$ cm, while $h_s = 5$ cm is length of the bolts. The bolt area is taken equal 25 cm^2.

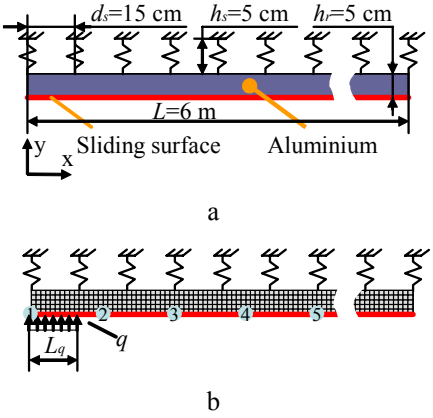

Fig. 3 2D model of the rail gun: a – geometry and supports; b – FE model with loading and specified nodal points

Fig. 3, b illustrates the finite element model comprising finite element mesh and applied loads. The final element mesh consists of 12305 2D plane elements. Connection bolts are approximated by 60 elastic spring elements. The whole model includes 26911 degrees of freedom. The load is defined as normal pressure acting on the rail.

The rail is made of aluminium, while the bolts are fabricated from steel. Material properties employed in numerical tests of the rail gun are given in Table.

Table

Material properties

	Material	Physical properties
Rail	Aluminium	Density: ρ =2.75 g/cm^3 Elast. modulus: E = 68.95 GPa Poisson's ratio: ν =0.3
Bolt	Steel	Density: ρ =7.8 g/cm^3 Elast. modulus: E =206.85 GPa Poisson's ratio: ν =0.3

3.2. Moving loads

In this work, transversal time-dependent loading of rail reflecting projectile load force is considered. The

profile of moving load is nearly uniform in space (Fig. 4, a). The sine shaped beginning and end of the impulse assumed in order to avoid local concentration. Length of the loaded surface $L_q = 15$ cm. Time variation of the load is defined as the loading impulse with maximal pressure $q = 100$ kPa or resultant loading force, acting on the rail $F_N = 750$ N. Load character at several characteristic points is presented in Fig. 4, b.

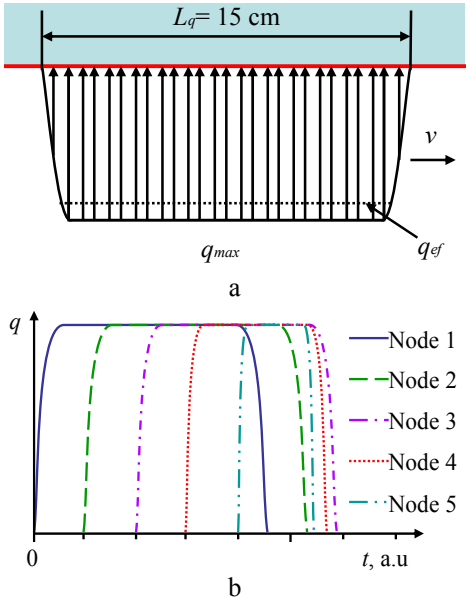

Fig. 4 Illustration of moving load: a – load distribution in space; b – time variation of the load in specified nodes

The rail was loaded by uniformly accelerating impulse. The position x_f and velocity v of the load front is defined by standard laws

$$x_f(t) = x_0 + v_0 t + \frac{at^2}{2} \tag{15}$$

$$v(t) = v_0 + at \tag{16}$$

Here, x_0 is initial position equal 0 m; v_0 is initial velocity equal 500 m/s; a is acceleration equal 400000 m^2/s; t is time variable. The load velocity becomes equal 2273 m/s at the end of the rail, when t = 4.43 ms. Eqs. (15), (16) provide unique definition of moving load in the investigated time interval. Considering linear dependency between load velocity and time we could examine moving load as the function of the velocity instead of the function of time. The considered approach is very convenient for investigating dependency of friction ratio factor on the velocity.

The load profile is defined by the following formula

$$q(l_r) = \begin{cases} 0, & \text{if } 0 > l_r \text{ or } l_r > 1 \\ q \sin\left(\frac{\pi}{2}\frac{l_r}{0.05}\right), & \text{if } 0 \le l_r \le 0.05 \\ q, & \text{if } 0.05 < l_r \le 0.95 \\ q \sin\left(\frac{\pi}{2}\frac{(l_r - 0.95)}{0.05}\right), & \text{if } 0.95 < l_r \le 1 \end{cases} \tag{17}$$

where l_r is reduction length

$$l_r(x, x_f) = \frac{(x - x_f)}{L_q} \tag{18}$$

The profiles of moving load are computed in preprocessing program MOVLOAD written by using object oriented programming language C++. The resulting values of the nodal loads are stored in macro file considering native ANSYS format. The file includes information on all load steps for each time instant. Macro files are loaded by command EXECUTE MACRO finishing interactive stage of specific pre-processor MOVLOAD and FEM software ANSYS. The pre-processor automatically computes values of the nodal loads and significantly reduces time for data preparation.

4. Numerical results and discussions

Investigation of the friction phenomenon in the rail gun is provided by considering time history of the rail displacements. Two-dimensional illustration of the characteristic parameter normal contact displacement of the space u_y is presented in Fig. 5, where the colour of each point indicates the value of displacement of point x in time t. Positive displacement is coloured by light grey colour, while negative displacement is plotted by dark grey colour.

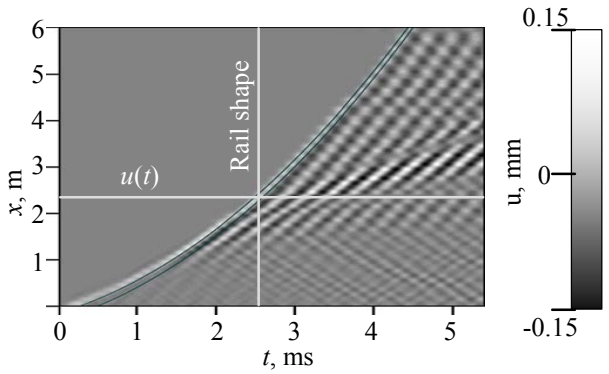

Fig. 5 Two-dimensional illustration of time history of normal contact displacement

The picture clearly illustrates the zero displacement region located in the area near the left upper corner. Such an area was rendered by the uniform grey colour. The interregional boundary coincides with parabola indicating initial position of the load. The remainder region of the graphs exhibits the motion of displacement waves. This region may be conditionally divided into several subregions indicating different character and different magnitudes of the displacement field, while complex pattern may be explained by the existence of resonance velocities.

Two characteristic longitudinal and time variations of the normal displacements are given for the sake of illustration. Any cross-section parallel to the x axis illustrates the shape of the rail at the particular time t. Deformed shapes of the rail at selected time instances t = 1.35 ms, t = 2.51 ms, t = 3.51 ms and t = 4.00 ms are presented in Fig. 6. The dots relevant to each graph indicate position of the moving load. The graph at t = 2.51 ms corresponds to the vertical white line illustrated in Fig. 5.

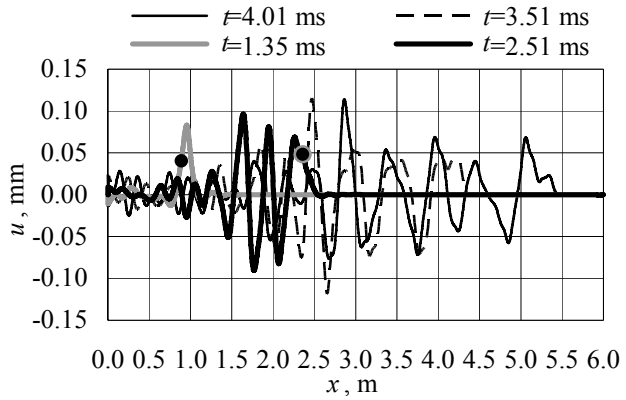

Fig. 6 Vertical rail displacements at different time moments

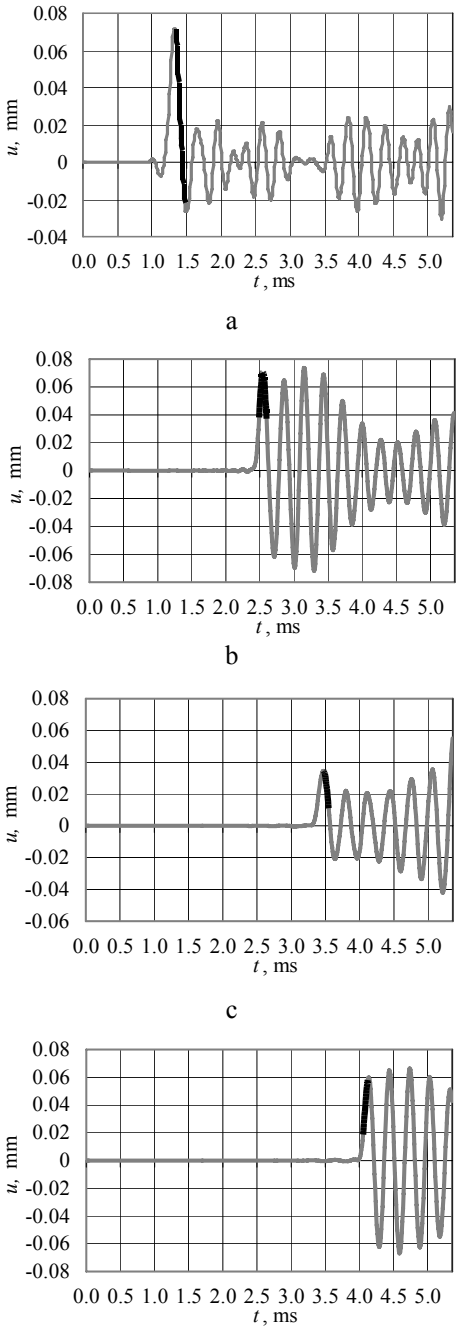

Fig. 7 Time histories of the various nods displacements: a – for point $x = 0.89$ m; b – for point $x = 2.36$ m; c – for point $x = 4.07$ m; d – for point $x = 5.23$ m

If should be noted that ordinates of the dots correspond to displacements under load used for evaluation of friction ratio.

Any cross-section of plot (Fig. 5) parallel to the t axis represents time history of displacements at particular rail node with coordinate x. Fig. 7 shows time history of averaged displacements of the nodes $x = 0.89$ m, $x = 2.36$ m, $x = 4.07$ m and $x = 5.23$ m. The term "averaged" stands for average displacement obtained by integration of nodal displacement over the loaded area L_q. The bold lines indicate loading history of node subjected by moving load in the time interval between two parabolas. The graph at, $x = 2.36$ m is indicated by the white horizontal line in Fig. 5.

The friction ratio is directly computed according to Eq. (10) from the displacement histories. In Fig. 8, the dependency of the friction ratio factor on the projectile velocity is illustrated. Here, the numerical values of η_1 is computed by using Eq. (12) for contact displacement u_N, η_2 is obtained by using Eq. (13), while η_3 is evaluated by using Eq. (14). The largest values of the factors computed in three different ways are observed at the critical velocities.

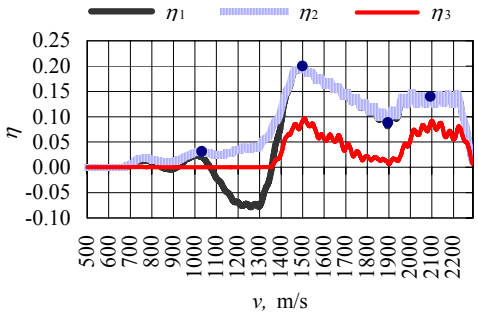

Fig. 8 The friction ratio factors η_1, η_2, η_3 computed by using different approaches according to Eqs. (12), (13) and (14)

The suggested friction indicators actually presents envelope of displacement histories and reflect dynamic nature. The total contact energy approach model (13) provides the highest values reflecting energy loses during brush contact. Maximum of the friction ratio factor is obtained at $v = 1507$ m/s, which could be treated as the resonance value. Other extremum is observed at the velocity equal to 2100 m/s.

5. Concluding remarks

Evaluation of friction in the rail gun under accelerating loading is illustrated by the dynamic finite element analysis. It was found that time variation of the friction ratio factor reflects dynamic behaviour of the rail capturing resonance related to critical velocities. Comparison of different contact area approaches exhibited that the full contact approach corresponding to brush sliding friction obtains the highest friction ratio values. The time history of friction ratio actually presents the envelope of the averaged normal dynamic contact displacements.

However, experimental validation would be desirable. The advantage of this approach is that friction influence could be evaluated by relatively simple processing of displacements.

References

1. **McNab, I.R.** Advances in Electrical Current Collection. -New York: Elsevier Sequoia, 1982, -327 p.
2. **Ross, D.P., Ferrentino, G.L.** Experimental determination of contact friction for an electromagnetically accelerated armature. -Wear 78, 1982, p.189-200.
3. **Craddock, W., Virostek, S., Calvin H., Eljes Y.** Thermal analysis of fiber armatures. -IEEE Transactions on Magnetics, 1989, No25(1), p.127-132.
4. **Aigner, S., Igenbergs, E.** Friction and ablation measurements in a round bore railgun.-IEEE Transactions on Magnetics, 1989, No25(1), p.33-39.
5. **Lehmann, P., Peter, H., Wey J.** Experimental study of solid armatures for eml applications.-IEEE Transactions on Magnetics, 1993, No29(1), p.848-852.
6. **Urukov, B.A., Lebedev, A.D., Milyaev, C.C.** Influence of materials properties on the dynamics of metal armature acceleration in a railgun.-Proc. of the 4 European Symposium on Electromagnetic Launch Technology, 1993, p.153-158.
7. **Khandryga, D.V., Plekhanov, A.V, Tereschenko, A.N.** Numerical simulation and experimental results of the metal armature acceleration.-IEEE Transactions on Magnetics, 1995, No31(1), p.193-197.
8. **Rodger, D., Lai, H.C.** A comparison of formulation for 3D finite element modelling of electromagnetic launchers. -IEEE Transactions on Magnetics, 2001, No37(1), p.135-138.
9. **Fair, H.** The electromagnetic launch technology revolution.-Magnetics Magazine, Webcom Communication, 2003, p.12-14.
10. **Barber, J., Bauer, D., Jamison, K., Parker, J., Stefani, F., Zielinski, A.** A survey of armature transition mechanisms. -IEEE Transactions on Magnetics, 2003, No39(1), p.47-51.
11. **Gallant, J., Lehmann, P.** Experiments with brush projectiles in a parallel augmented railgun. -IEEE Transactions on Magnetics, 2005, No41(1), p.188-193.
12. **Tzeng, J.T.** Structural Mechanics for electromagnetic railguns, -IEEE Transactions on Magnetics, 2005, No41(1), p.246-250.
13. **Johnson, A.J., Moon, F.C.** Elastic waves and solid armature contact in electromagnetic launchers. -IEEE Transactions on Magnetics, 2006, No42(3), p.422-429.
14. **Novickij, J., Stankevič, V., Balevičius, S., Žurauskienė, N., Cimmperman, P., Kačianauskas, R., Stupak, E., Kačeniauskas, A., Löffler, M.J.** Manganite sensor for measurements of magnetic field disturbances of pulsed actuators. -Solid State Phenomena, 2006, v.113, p.459-464.
15. **Barber, J.P, Challita, A.** Velocity effects on metal armature contact transition. -IEEE Transactions on Magnetics, 1993, No29(1), p.733-738.
16. ANSYS Theory Reference, 8 edition, SAS IP INC., 2003.-786p.

L. Tumonis, R. Kačianauskas, A. Kačeniauskas

BĖGIO DEFORMACIJA SUKELTOS TRINTIES VERTINIMAS ELEKTROMAGNETINĖJE ŠAUDYKLĖJE: SKAITINIAI TYRIMAI

R e z i u m ė

Baigtinių elementų metodu tirta elektromagnetinės šaudyklės, veikiamos tolygiai greitėjančia apkrova, bėgio dinamika ir trintį lemiantys rodikliai. Sviedinio ir bėgio kontaktas nagrinėjamas supaprastintai, pakeičiant sviedinio poveikį žinoma judančia apkrova. Judančios apkrovos sukeltam trinties padidėjimui vertinti pasiūlytas bematis trinties rodiklis, kurį lemia kontaktinio paviršiaus normaliniai poslinkiai.

L. Tumonis, R. Kačianauskas, A. Kačeniauskas

EVALUATION OF FRICTION DUE TO DEFORMED BEHAVIOUR AT RAIL IN THE ELECTROMAGNETIC RAILGUN: NUMERICAL INVESTIGATION

S u m m a r y

The dynamic behaviour and evaluation of friction due to deformed behaviour of rail in the electromagnetic rail gun under accelerating loading are investigated by using the finite element method. The simplified uncoupled rail-projectile contact model is applied, where action of the projectile is described as given moving loading. The dimension-less friction ratio is suggested to evaluate the increase of the friction during motion of the load.

Л. Тумонис. Р. Качянаускас А. Каченяускас

ОЦЕНКА ТРЕНИЯ, ВОЗНИКАЮЩЕГО ПРИ ДЕФОРМАЦИИ РЕЛЬСА, В ЭЛЕКТРОМАГНИТНОЙ РЕЛЬСОВОЙ ПУШКЕ: ЧИСЛЕННОЕ ИССЛЕДОВАНИЕ

Р е з ю м е

Методом конечных элементов исследовались динамика и показатели трения рельсовой пушки, находящейся под действием ускоряющейся нагрузки. Применялась упросчённая модель контакта снаряда и рельса, где воздействие снаряда представлена как двигающаяся нагрузка. Для исследования увеличения силы трения, возникающей из-за двигающейся нагрузки, был предложен безразмерный показатель трения, зависящий от нормальных смещений.

Received October 19, 2006